Science of the Total Environment 883 (2023) 163397

Contents lists available at ScienceDirect

Science of the Total Environment

journal homepage: www.elsevier.com/locate/scitotenv

Influence of local scale and oceanic teleconnections on regional fire danger and wildfire trends

Flavio Justino [a,*], David H. Bromwich [b], Sheng-Hung Wang [b], Daniel Althoff [c], Vanucia Schumacher [d], Alex da Silva [e]

[a] Department of Agricultural Engineering, Universidade Federal de Vicosa, PH Rolfs, Vicosa, Brazil
[b] The Ohio State University, Byrd Polar and Climate Research Center, 108 Scott Hall, 1090 Carmack Rd, Columbus, OH 43210, USA
[c] Department of Physical Geography, Bolin Centre for Climate Research, Stockholm University, Stockholm, Sweden
[d] Instituto Nacional de Pesquisas Espaciais, São José dos Campos, São Paulo, Brazil
[e] Universidade Federal do Oeste do Pará, Instituto de Engenharia e Geociências, Santarem, PA, Brazil

HIGHLIGHTS

- Global wildfires incidence is tightly dependent on Atlantic SST.
- Maximum PFI matches 80 % of observed fires.
- Fire impact of short-term precipitation is dependent on local vegetation.

GRAPHICAL ABSTRACT

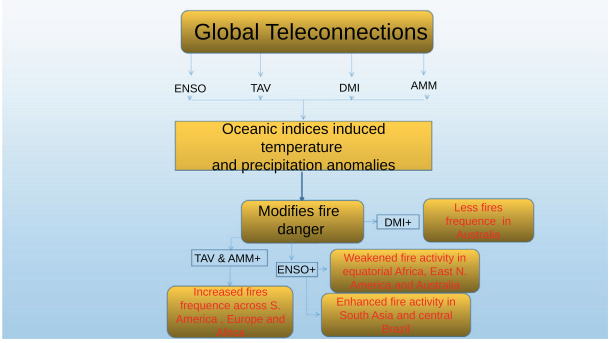

ARTICLE INFO

Editor: Paulo Pereira

Keywords:
Teleconnections
Fire weather index
Potential fire index
Drought
Oceanic climate modes

ABSTRACT

Studies and observations have pointed out that recent wildfires have been more severe and burned area is increasing in tropical regions. The current study aims at investigating the influence of oceanic climate modes and their teleconnection on global fire danger and trends in the 1980–2020 interval. Disentangling these trends demonstrates that across the extratropics they are primarily related to increases in temperature, whereas in the tropics changes in short-term precipitation distribution dominates the trends. Moreover, the environmental impact of short-term precipitation is dependent on local vegetation type and tightly related to oceanic temperatures far from the burned areas. Indeed, in the 2001–2020 period, a warmer tropical North Atlantic was associated with more fires in the Amazon and Africa, whereas ENSO has weakened the fire activity in equatorial Africa. The remarkable impact of oceanic modes of climate variability in inducing environmental conditions conducive to fires, has particular relevance for the seasonal spatiotemporal wildfire forecasts. Although local aspects are crucial for fire management, long-term predictions should take into account the behavior of potential climate drivers located far from the region of interest. Such teleconnections can be identified ahead of local weather anomalies.

1. Introduction

Shifts of local climate and weather are associated with surface conditions and oceanic far-reaching disturbances (Liu and Alexander, 2007). Increased deforestation and urbanization are associated in most cases with local higher temperatures and more frequent torrential rains (Chapman

* Corresponding author.
E-mail address: fjustino@ufv.br (F. Justino).

http://dx.doi.org/10.1016/j.scitotenv.2023.163397
Received 16 November 2022; Received in revised form 30 March 2023; Accepted 5 April 2023
Available online 17 April 2023

et al., 2017; DeFries et al., 2010). Notwithstanding, fluctuations of oceanic characteristics originated far from a particular region play an important role to anomalous climate conditions elsewhere, known as teleconnections (Wallace and Gutzler, 1981).

Fires have been in the forefront of global issues due to their influence on ecosystem dynamics and population welfare. Earl and Simmonds (2018) investigating spatial and temporal variability of fire found a decline in active fires globally, but regional analyses demonstrated increased fire activity in China and India due to rapid agricultural intensification. Elucidation of drivers of the recent increase in wildfire destructiveness and frequency, urges interdisciplinary strategies involving weather monitoring and necessary land surface management. Attribution of causes have frequently been associated with increased temperature linked to global warming, changes in ocean/atm teleconnections and deforestation related to the expansion of agricultural activities (Zhao et al., 2022; Wang and Cai, 2020; Shi and Touge, 2022).

Surprisingly, the medium-term effect of droughts and dry spells on regional and local fire has not been properly estimated, which frequently lead to misrepresentation of regional vulnerability to fires (Richardson et al., 2022). Limited understanding and fire forecast skill arise from assuming that reduced fire danger and lower probability of fires, result from occurrences of precipitation within an individual day or short-time period. Instead, efforts should be made to characterize in detail changes in the temporal distribution of precipitation, and how those changes interact with vegetation to produce combustible material necessary for fire initiation.

Urban and rural localities have been affected by local or distant wildfire (Iglesias et al., 2022; Karanasiou et al., 2021) events, which include forest, agricultural and bush fires. The overall consensus is that higher tropospheric temperatures increase the frequency of large fires by modifying vegetation characteristics due to reduced soil and plant moisture (Le Page et al., 2015; Justino et al., 2022). Indeed, analyses of temperature evolution during the recent decades exhibit an upward warming trend, with large values in particular across the subtropical and extratropical latitudes of the Northern Hemisphere (Ades et al., 2020). Tian et al. (2022) argued that forest fires contribute to 60 % of the total fire counts in Northern Eurasia, whereas cropland contributing to 66 % of the decrease trend across southwestern part.

Nonetheless, vegetation greening/browning is dominated by radiation in rainforest zones, by precipitation in arid and semiarid areas, and by temperature at high latitudes (Blok et al., 2011; Wu et al., 2015; Nemani et al., 2003). Hence, the sensitivity of vegetation to temperature should be analysed locally due to plant type characteristics, and their response to the thermal forcing. Estimates of past, current or future fire behavior and danger based solely on temperature do not depict the global picture and may lead to misinterpretation without including daily precipitation distribution (Justino et al., 2022).

Unfavorable intraseasonal and interannual variability of precipitation lead to higher vulnerability to fire across forest, grassland, savannas, tundra, and shrub-lands, with respect to estimates solely based on the vegetation response to temperature (Lasslop and Kloster, 2017). Because the frequency of precipitation as measured by number of rainy days substantially advances the leaf onset date (Wang et al., 2022b), the amount of ignition sources increases during the fire season.

Methods to estimate fire weather danger have efficiently identified fire-prone regions, and major efforts have been spent to quantify the individual contributions of weather variables to fire danger (Jain et al., 2021; Zhang et al., 2021; Da Silva et al., 2021; Dowdy et al., 2010). Surface temperature and relative humidity have been responsible for trends in Fire Weather Index (FWI) (Van Wagner and Forest, 1987). For almost half of the Earth's burnable surface, according to Jain et al. (2021). This conclusion should be viewed with caution because the attribution of the dominant cause of increased fire danger to temperature and humidity may neglect the crucial role of daily and intra-seasonal distribution of precipitation (Varga et al., 2022). The FWI system includes daily precipitation as an input to calculate three fuel moisture codes at different soil depths (representing dead fuel moisture). This also accounts for intra-seasonal variations in precipitation and the cumulative effects of long term drought through the drought code which has a long equilibrium drying time (53 days) (Van Wagner and Forest, 1987).

Observed hotspots have been found across regions dominated by low fire danger northward of 40°N, due to drawbacks in FWI for representing the vegetation-precipitation relationship (Justino et al., 2021). The scale of attributing the magnitude of the fire danger in FWI, leads for instance in the Balkans/central Asia to fires within FWI lower the 25 (Justino et al., 2021), and this does not contribute to have a reasonable fire forecast.

The FWI was originally designed for a standard pine forest in boreal latitudes (Van Wagner and Forest, 1987), and other biomes are not well sampled. This limitation in FWI has been partially alleviated by the Potential Fire Index (PFI) that takes into account the role of different vegetation types and time evolving precipitation in the preceded 120 days (Justino et al., 2011; Da Silva et al., 2021). The PFI is able to identify regions prone to fire development, as demonstrated by the satellite detected-fire in the 2001–2016 interval. It is found that PFI delivers an efficiency by up to 80 % in matching the observed fires from Terra/MODIS satellite (Da Silva et al., 2021).

The current study investigates the main causes of fire weather trends from 1980 to 2020 based on fire weather indices, meteorological variables, satellite-based hotspots and burned areas. The relationship between fire danger and fire occurrences with large-scale oceanic modes are also explored in detail. The far-reaching effect of anomalous patterns of large-scale climatic modes of variability affect the burned area and the incidence of fires substantially (Shi and Touge, 2022; Le Page et al., 2008; Jolly et al., 2015). Therefore, past and present influences of El-Niño-Southern Oscillation (ENSO), the Atlantic Ocean variability for instance, are analysed to elucidate changes in the fire season, contributing to foresee future extreme fires even in areas not currently affected.

2. Methods and data

The Climate Prediction Center (CPC) dataset, which includes weather stations and several additional observational data for precipitation and temperatures, has been chosen for the PFI calculation because Da Silva et al., 2021 demonstrated higher capability of this index to reproduce regions with observed fires, in comparison to similar calculations based on ERA5. It should be emphasized that no differences are noted by comparing the regions with higher PFI based on CPC and ERA5. All dataset currently utilized here are interpolated to the 0.5 × 0.5°. Slight differences are found only in the magnitude values. However, the ERA5 relative humidity is currently used because this variable is not available in the CPC datasets. After downloading the datasets, the Climate Data Operators (CDO) and NCAR command Language (NCL) have been applied to compute the PFI on daily basis. The ERA5 hourly data on pressure levels from 1980 to 2020 data has been downloaded from https://cds.climate.copernicus.eu/cdsapp!/dataset/. Both datasets have been retrieved in February 2022.

The FWI system (https://cds.climate.copernicus.eu/) provides fire danger information following the European Forest Fire Information System (EFFIS) based on the ERA5 dataset. Additional details on FWI characteristics may be found at https://cwfis.cfs.nrcan.gc.ca/background/summary/fwi. The FWI is categorized as such: very low (0.0–5.2), low (5.2–11.2), moderate (11.2–21.3), high (21.3–38.0), very high (38.0–50.0) and extreme (50.0–100.0).

2.1. PFI fire danger

The PFI has been described in other studies (Justino et al., 2021, Justino et al., 2011; Da Silva et al., 2021) and for brevity detail is not provided here. Several equations are applied to parameterize temperature (FT), precipitation and the vegetation cover response of these quantities as drivers for the PFI. The FT takes into account temperature, such as shown by the equation below:

$$FT = [0.02 \times Tm + 0.4) \times (0.003|Lat|+1)] \quad (1)$$

where, Tm is the mean temperature and |Lat| stands for the grid latitude in degrees. The FT is included as a fire danger factor because similar air temperatures in the tropics and extra-tropics are associated with distinct vegetation responses, and thus fire danger.

A different factor has been included to replace the LogHai (Justino et al., 2022): This is implemented, because LogHai requires air temperature and dewpoint temperatures from surface to 700 hPa to estimate the effect of relative humidity and atmospheric instability on PFI. The relative humidity (r) influence on PFI is measured by Eq. (2) below.

$$FU = (- 0.006 \times r) + 1.3 \quad (2)$$

It increases when humidity is <50 % and diminishes for values >50 % (Justino et al., 2011). FT and FU are combined to reproduce the impact of changes in temperature and atmospheric humidity on the fire danger, namely FTU = FU × FT. These changes do not lead to substantial differences of PFI values as compared to previous results (Da Silva et al., 2021). To clarify the sequence of calculations a flowchart has been added to Supplementary material (Fig. S1).

The PFI also takes into account the type, and natural cycle of vegetation defoliation, which is represented by considering the link between the vegetation and the precipitation distribution as a sine function (Justino et al., 2021). The vegetation data used is generated from annual MODIS MOD12C1 (https://lpdaac.usgs.gov/products/mcd12c1v006) and MCD12Q1 (https://lpdaac.usgs.gov/products/mcd12q1v006/) product observations, available from the Land Processes DAAC.

2.2. Satellite-derived fire activity

The processed Moderate Resolution Imaging Spectroradiometer (MODIS) Collection 6 Near Real-Time (NRT) active fire products (Aqua + Terra) based on the standard MOD14DL/MYD14 fire and thermal anomaly algorithms have been used as fire proxies (Giglio et al., 2016). These data are available at https://earthdata.nasa.gov/earth-observation-data/near-real-time/firms (last access:

February 2022). The MODIS hotspots (MCD14DL) are downloaded at 1 km resolution from 2001 to 2020. Statistical analyses on these data and their association to climate conditions have been provided in previous publications (Justino et al., 2022; Da Silva et al., 2021). MODIS active fires are detected during the satellite passage and not necessarily all fires are captured because hotspots with lower intensity can be extinguished at that particular time. Moreover, detection rates increased with fire size.

2.3. Burned area

Major effort has been spent to compute Earth burned areas used in this study. This is derived from the MODIS/Terra + Aqua combined MCD64A1 Version 6 Burned Area data product. The MCD64A1 is a monthly, global gridded 500-m product providing the estimated day of year (1 to 366), when burning has been detected, from November 2000 to present. The MCD64A1 database was retrieved on January 9, 2022, from https://lpdaac.usgs.gov/products/mcd64a1v006/, maintained by the NASA EOSDIS Land Processes Distributed Active Archive Center (LP DAAC) at the USGS Earth Resources Observation and Science (EROS) Center, Sioux Falls, South Dakota. A total of 67,536 images comprising the period from 2000 to 11-01 to 2021-10-01 (252 months and 268 images/month) have been downloaded. The pixels from the monthly burn day of the year product are classified just as unburned or burned areas (0 or 1) for the corresponding month. Images are first re-projected to the WGS 84 coordinate reference system (EPSG:4326) and aggregated to a spatial resolution of 0.5° x 0.5°. The 268 images/tiles of each month are then combined (mosaiced) resulting in a monthly global dataset (longitude: 0° to 360°, latitude: 60°S to 70°N), containing the percentage of area burned per pixel.

The total area burned per pixel was obtained by multiplying the percentage of burned area per pixel equivalent area.

2.4. Global climate indices

Empirical Orthogonal Function analyses (EOF) have been utilized to compute global oceanic indices based on monthly averages of ERA5 Sea Surface Temperatures, spanning the 1980–2020. The EOF is applied to compute the El-Niño-Southern Oscillation (ENSO, 20°S-20°N, 160°W-80°W), Atlantic Meridional Mode (AMM, 20°S-32°N, 75°W-15°E) and the Atlantic tripole (Atl-Tripole, 10°N-70°N, 80°W-0°), according to definitions available at https://psl.noaa.gov/data/climateindices/list/.

The Dipole Mode Index (DMI) and Tropical Atlantic Variability (TAV) are based on SST regional differences. The TAV and DMI are also calculated based on ERA5 SST. The DMI indicates the east-west temperature gradient across the Indian Ocean (Black et al., 2003), between the eastern (10°S–0°, 90°–110°E) and western (10°S–10°N, 50°–70°E) basins. The TAV displays differences between SST anomalies in the tropical Atlantic between 5.5 N°-23.5°N, 15 W-57.5°W and Eq-20°S, 10°E-30°W.

3. Results and discussion

3.1. Fire weather danger distribution

The Potential Fire Index (PFI) and FWI are initially analysed based on daily data and compared with distribution of precipitation and temperature in the spatiotemporal domain. Moreover, their ability to reproduce regions which experience high number of fires is also verified (Fig. 1a-d).

Limitations in FWI may be demonstrated by comparing its time mean conditions from 1980 to 2020, with the PFI (Fig. 1a,b). The FWI shows reduced areas with higher fire vulnerability in regions that experience frequent burning, such as South America, western North America and most of Eurasia (Figs. 1a,b and 2 in Supplementary Material S2). It has to be mentioned that the satellite based-hotspots span 2001 to present. In PFI >85 % (70 %) of satellite-based fires in the tropics (middle-latitudes, 30°N-45°N), between 2001 and 2020, are found in moderate-high fire danger zones (PFI > 0.5), whereas in FWI this correspondence is drastically weakened, as shown in Figs. 1c,d and S3 b. Most fires are categorized in FWI under low and moderate risk (FWI < 25). The FWI ranging between 21.3 and 38.0 is classified as high risk of fire, thus, most fires should be found under these values.

Fig. 1e,h show 7-day averaged correlation throughout the 1980–2020, between the PFI/FWI and the period of drought (DD) and parameterized air temperature, as represented by the factor of temperature (FT). The DD is defined as the temporal evolution of precipitation in distinct intervals during the preceding 120 days (Da Silva et al., 2021). There are highly significant values in PFI related to DD in the tropics, and related to temperature in the extratropics. This correlation pattern fits nicely with results that demonstrate how vegetation responds to changes in weather variables (Dowdy et al., 2010). It should be mentioned that there is high 7-day correlation at lag 0 between DD and FT over western North America, northern South America, equatorial Africa, and southern Australia, where both factors contribute in phase to increase the fire danger, with dry and warm conditions. Turning to FWI correlations (Fig. 1f,h) much lower correlation values are found in comparison to PFI. Despite being statistically significant, those values are lower than 0.4 demonstrating that the FWI heavily relies on relative humidity and wind speed (Jain et al., 2021), instead of precipitation distribution. It should be noted that the DD and FT are components of the PFI, so the correlation would be expected to be better than with another index that uses temperature and precipitation information differently.

3.2. Trends in fire danger and their link with weather variables

To verify the consistency of both indices, Fig. 2a,b show the 40-year annual trends of FWI and PFI based on daily averaged values (positive values indicate an increase in environmental fire vulnerability). The calculation includes all values delivered by the FWI and PFI, and despite large similarities over western North America and western Eurasia, very different

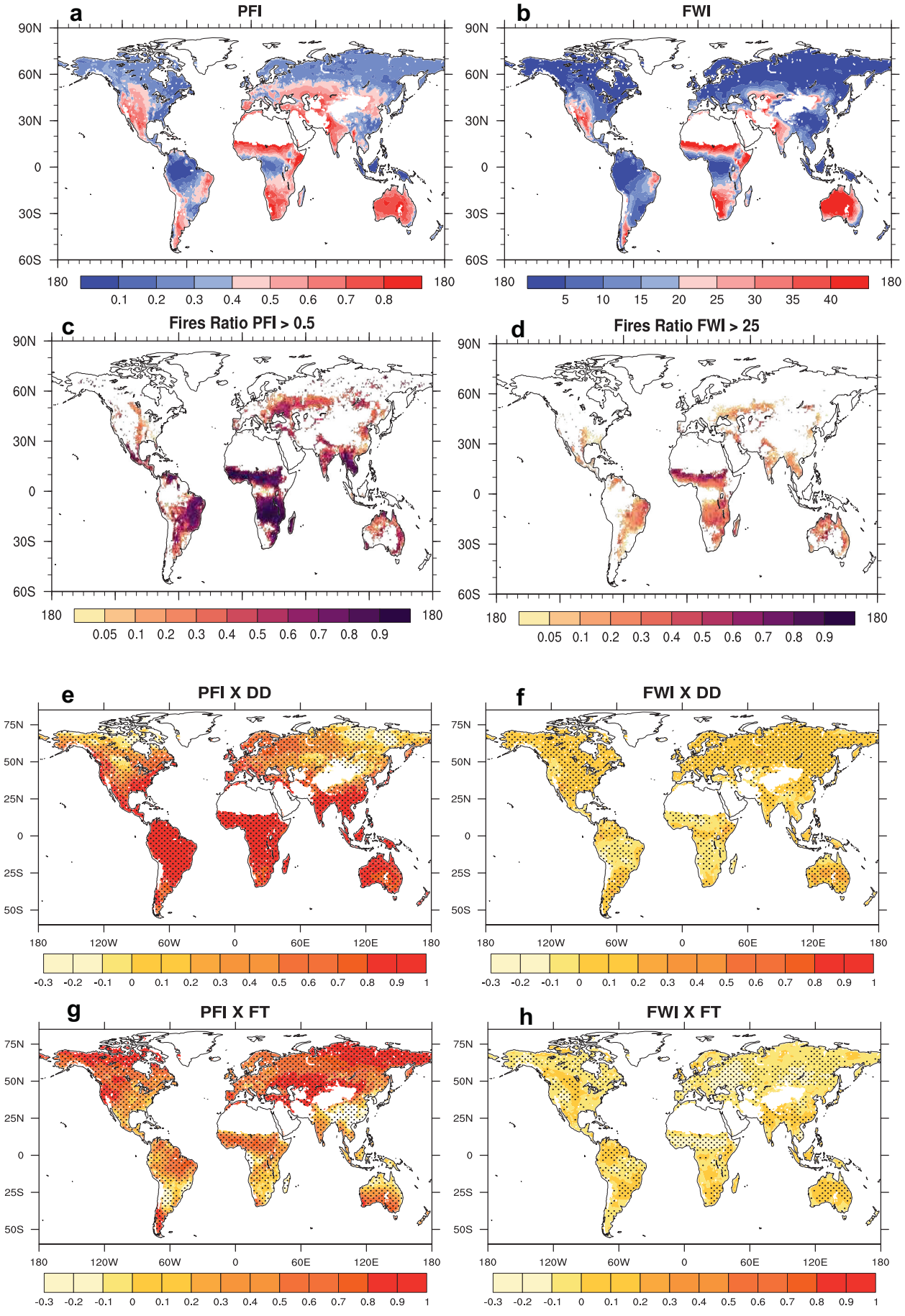
a
PFI
90N
60N
30N
0
30S
60S
180
180
0.1 0.2 0.3 0.4 0.5 0.6 0.7 0.8
b
FWI
90N
60N
30N
0
30S
60S
180
180
5 10 15 20 25 30 35 40
c
Fires Ratio PFI > 0.5
90N
60N
30N
0
30S
60S
180
180
0.05 0.1 0.2 0.3 0.4 0.5 0.6 0.7 0.8 0.9
d
Fires Ratio FWI > 25
90N
60N
30N
0
30S
60S
180
180
0.05 0.1 0.2 0.3 0.4 0.5 0.6 0.7 0.8 0.9
e
PFI X DD
75N
50N
25N
0
25S
50S
180 120W 60W 0 60E 120E 180
-0.3 -0.2 -0.1 0 0.1 0.2 0.3 0.4 0.5 0.6 0.7 0.8 0.9 1
f
FWI X DD
75N
50N
25N
0
25S
50S
180 120W 60W 0 60E 120E 180
-0.3 -0.2 -0.1 0 0.1 0.2 0.3 0.4 0.5 0.6 0.7 0.8 0.9 1
g
PFI X FT
75N
50N
25N
0
25S
50S
180 120W 60W 0 60E 120E 180
-0.3 -0.2 -0.1 0 0.1 0.2 0.3 0.4 0.5 0.6 0.7 0.8 0.9 1
h
FWI X FT
75N
50N
25N
0
25S
50S
180 120W 60W 0 60E 120E 180
-0.3 -0.2 -0.1 0 0.1 0.2 0.3 0.4 0.5 0.6 0.7 0.8 0.9 1

patterns are noticed across Asia, where most negative trends delivered by the PFI oppose positive values in FWI (Fig. 2a,b).

This further indicates the secondary role of precipitation in FWI (Fig. 2c). Indeed, the impact of precipitation distribution is very limited in the FWI leading to an overestimation of the temperature contribution to fire danger (Fig. 2b,d).

Additional analyses are performed to verify trends in extreme fire danger values, as represented by the 90th percentile (90p, Fig. 2e,f). Positive trends of the 90p show that severe fire weather conditions above this threshold have become more frequent during the 1980–2020 (Fig. 2e,f). Severe fire weather conditions are increasing globally, in particular across sub-Saharan Africa, eastern Australia, South America and western North America (Fig. 2e,f), and temperature is responsible for increasing fire danger over Alaska and western Russia/east Europe (Fig. 2d). It can be argued that precipitation plays less of a role for the extreme conditions, because the DD 90p shows much larger blue regions than the PFI 90p maps, and the FWI and PFI 90p agree better than their means.

In Asia and Africa, however, the dominant effect of DD distribution in reducing fire danger is not depicted by the FWI, that mostly shows positive trends over those regions. By weakening the impact of precipitation, the FWI may misrepresent future fire danger estimates based on climate simulations as part of the Coupled Model Intercomparison Project (CMIP). The number of days with maximum values of PFI and FWI increases in many regions, as shown by statistically significant positive trends for the 90p (Fig. 2e,f). This indicates increased frequency in number of days with higher environmental vulnerability for fire occurrence, over areas that are currently affected by critical values in particular of PFI, such as western North America, South America, Europe-eastern Asia, Siberia and parts of Australia (Fig. 1a).

Attribution of causes for trends in the 90th percentile shows a latitudinal dependence, in the sense that temperature increases notably contribute to positive PFI and FWI between 40°N-70°N. The primary exception is central North America, where DD leads to negative trends in fire danger, and reduced frequency of occurrence of fire danger maxima (blue regions on Fig. 2a-f). In east Asia, the temperature effect (FT) dictates positive trends in the frequency of critical fire danger, despite increases in the number of days with higher accumulated precipitation (Fig. 2c,d). It turns out that the distribution amount of precipitation spanning the 120-day interval is not sufficient to oppose the warming effect. The remarkable role of short-term precipitation distribution to fire danger rating is depicted in Fig. 3. The combination between daily precipitation distribution and vegetation (Fig. 3a) is based on accumulated rainfall in distinct intervals during the preceding 120 days (F_p), the precipitation factor. This results in the period of droughts (DD) where $DD = 0.45\{1 + \sin[(A(F_p - 90)]\}$.

A is the vegetation flammability constant (Da Silva et al., 2021). The temporal evolution of DD is shown in Fig. 3b for northern California. Absence of precipitation increases DD as noticed by the sinusoidal growth which takes place from time 160. On the other hand, DD reduces as a sine function to approximately 0 when substantial amount of precipitation occurs (blue line, Fig. 3b).

It has to be stressed that similar values of DD result in distinct fire danger depending upon the background vegetation. Fig. 3 shows the fire danger component resulting from constant DD values (10, 30, 50) applied worldwide, but over distinct vegetation types. It is very clear that for DD = 10 environmental conditions are not prone to fire development (Fig. 3c), because vegetation is not dry enough to burn and the amount of fuel does not to support wildlfires. However, as soon as precipitation reduces, in frequency and volume, such as for DD = 30 or 50, fire danger increases according to the type of vegetation. Regions dominated by grassland, savannas and cropland (Fig. 3a) display danger ratings >0.8, and enlarged areas are noticed for DD = 50, leading to even higher fire danger ratings (Fig. 3c-e). Tropical forests are more resilient due to their capacity to collect water from subsurface soil layers, thus, they still experience lower fire danger for DD = 50. However, values of DD larger than 90 will induce high fire danger rating across these ecosystems.

3.3. Trends in fire danger and their link with oceanic climate modes

Trends in the fire regime are also associated with large-scale modes of climate variability. Previous studies have indicated that during the 2015/16 El Niño more fires have been detected worldwide (Burton et al., 2020). In Australia, burned area (BA) is also primarily controlled by extreme weather linked to fluctuations in the Dipole Mode Index (DMI) in the Indian Ocean (Wang et al., 2022a). Furthermore, it has been demonstrated that northern Africa's fire activity is highly influenced by tropical Atlantic Sea Surface Temperature (SST) during the dry season (November to March), and the tropical Indian Ocean during the wet season (April to September) (Yu et al., 2020). It is worth noting that more studies are needed on the influence of oceanic variability on the fire regime. Patterns of SSTs related to the Atlantic tripole (Atl-Tripole), Atlantic Meridional Mode (AMM), ENSO, DMI and the Tropical Atlantic Variability (TAV) influence fire frequency and destructiveness, because they induce precipitation and temperatures anomalies, modifying environmental characteristics far from their source regions.

In fact, these modes of climate variability influence the global climate by inducing teleconnections via atmospheric bridges. As discussed by Liu and Alexander (2007) and Alexander et al. (2002). The tropical impact on extratropical climate is accomplished mainly through the atmosphere. During ENSO events, the atmospheric response to SST anomalies in the equatorial Pacific influences the climate worldwide by leading to droughts in most of the tropics. Fluctuation of the TAV also induce meridional migration of the inter-tropical convergence zone (ITCZ), as well as modifies the Asian summer climate (Ratna et al., 2020), in particular tropical-extratropical and interhemispheric interactions. On the other hand, the extratropics interact with the tropics via the oceanic gyres.

Correlation analyses show that these modes are barely linked in time with ENSO, with exception of DMI that at lag 0 delivers a −0.35 correlation value, that is significant at 95 %. The Atlantic modes on the other hand are correlated such as that the AMM and Atl-Tripole correlation coefficient is 0.8, that is significant at 95 % and Atl-Tripole and TAV is −0.48, not significant at 95 %. The AMM and Atl-Tripole have similar global patterns but may be associated with different fire occurrences. Limitation arised due to the timeseries length that only span the years 1980–2020, which can impact the magnitude and significance of trends. However, society has been constantly affected by fire activity that emerges and is intensified by weather anomalies associated with global climatic drivers (Shi and Touge, 2022).

Fig. 4 shows the maximum lag-correlation and respective lag between the oceanic indices and the PFI. The maximum lag correlation (i.e., cross correlation) provides the maximum correlation coefficients between the indices and PFI, at the corresponding lag time. Maximum number of lags is 12 (months). In the current analyses the algorithm utilized by Song et al. (2019) based on the vector auto-regressive (VAR) model estimation has been used.

During the positive phases of the TAV and ENSO increased fire danger is found in Africa and northern South America, because these indices are associated with reduction of precipitation and consequently positive anomalies of DD (Fig. S2). Both regions, which are covered by tropical forests, are experiencing positive trends in fire danger with increased number of days with extreme values (Fig. 2e,f). Corroborating the positive ENSO-driven PFI anomalies, previous studies have demonstrated that fires have been more frequent and severe under positive ENSO events (Mariani et al., 2016; Harris and Lucas, 2019) (Fig. 4b). It is demonstrated that in the tropics maximum correlation between the TAV/ENSO and PFI occurs within

Fig. 1. Daily averaged (a) PFI and (b) FWI for the 1980–2020. (c) and (d) show the ratio of satellite-observed fires found under PFI and FWI classes larger than 0.5 and 25, and the 2001–2020 total accumulated fires. 7-day Pearson correlation for the 1980–2020 between (e) PFI and DD, and FWI and DD (f). (g) and (h) are the same as (e) and (f) but for the temperature factor (FT). Dotted regions are significant at 95\% level. Land regions with sparse or absent vegetation are shown in white, (a-b) and (e-h).

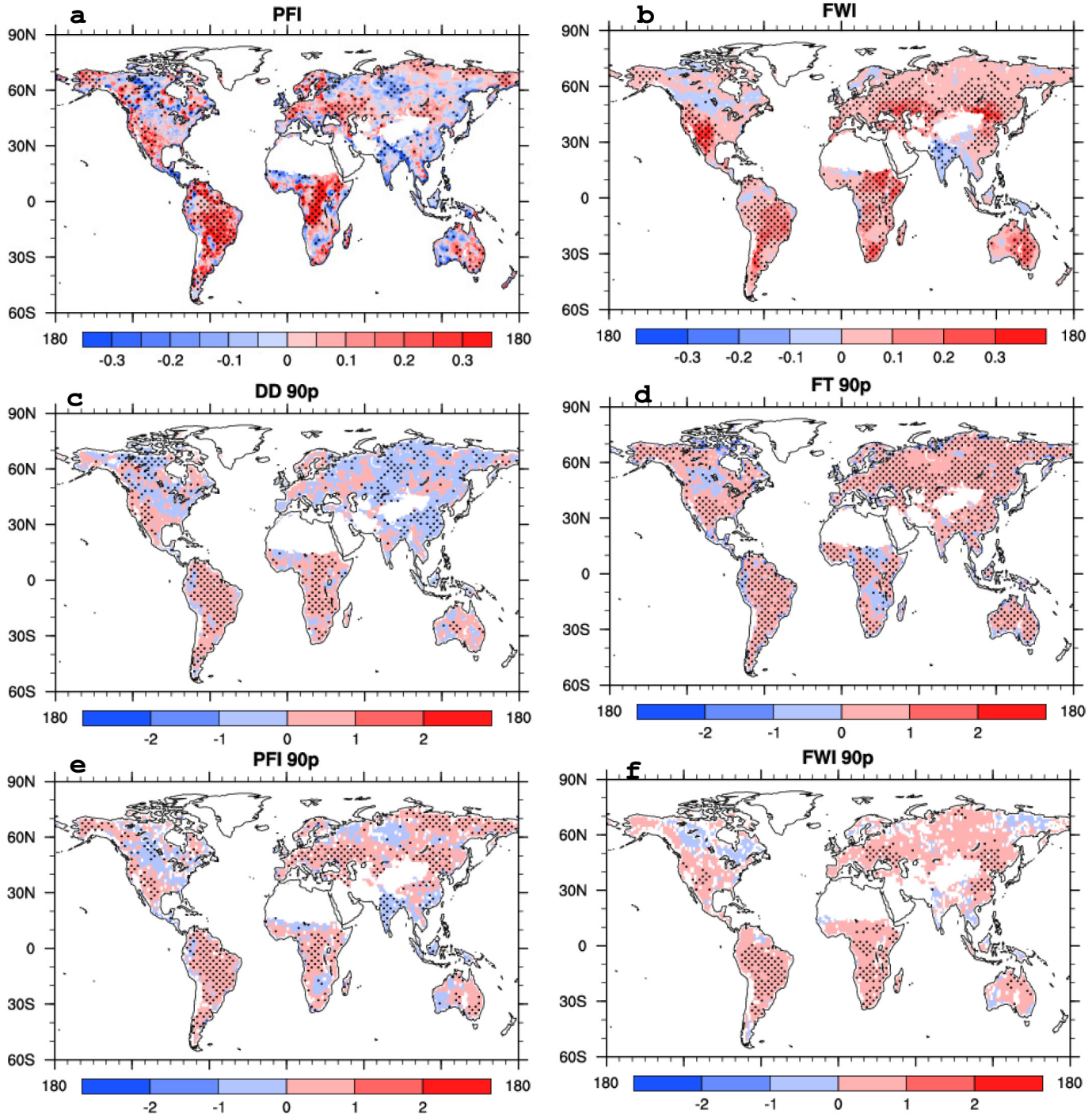

Fig. 2. (a) and (b) show annual Mann-Kendall trends based on daily values of PFI and FWI from 1980 to 2020. (c) and (d) show decadal Mann-Kendall 90 % percentile trends based on daily values of DD and FT (C). Patterns are displayed as increased (>0) or decreased (<0) number of days per decade. (e) and (f) are the same as (c) and (d) but for PFI and FWI. Dotted regions are significant at 95 % level. Land regions with sparse or absent vegetation are shown in white in (a-f).

the lags 0–3 months but at the equatorial region lags up to 6 months can be found (Fig. 4f,g). Briefly speaking, the effect of TAV and ENSO in the fire danger (PFI) is larger in the tropics where ENSO demonstrates larger impact with respect to the TAV. Across southern South America and Australia they have opposite effect, and the PFI response is related to the dominance of the index according to the lag. The impact of TAV in Australia (negative correlations) should be viewed with care, because more effort is needed to identify climate mechanisms governing the statistical correlation between TAV and PFI.

Across the extratropics maximum correlations related to ENSO (TAV) are larger for lags between 6 and 8 (0–3) months. Reduction in water availability during winter and spring of the year preceding the fire season has been found to be crucial for ignition during summer in southeast Australia (Harris and Lucas, 2019). Based on Mann-Kendall calculations, ENSO and TAV do not deliver statistically significant trends at 90 % level (Fig. 4f, Table 1). Nevertheless, a sequence of persistent events, such as positive ENSO or TAV is related to droughts in many regions (Gushchina et al., 2020), leading to substantial enhancement in fire danger. This is independent of long term trends. Persistent weather conditions related to TAV and ENSO have already been associated with increased number of fires worldwide, and in particular in the tropics (Burton et al., 2020; Fernandes et al., 2011).

Trends delivered by the DMI are statistically significant at the 90 % level (Table 1). The DMI influences the PFI in most of Australia and parts of South America, and southern Africa. In particular, the fire danger response is also in concert with the ENSO signal (Fig. 4b,c), but changes in the months of maximum correlation between ENSO and DMI differ in the Southern Hemisphere. The DMI greatly influences the PFI by 2–3 months ahead (Fig. 4h).

Turning to the Atlantic variability as indicated by the AMM and the Atl-Tripole, it is demonstrated that the PFI over South America and Africa is strongly affected by these indices (Fig. 4d,e). Indeed, the SST pattern of AMM and Atl-Tripole is characterized by an overall warming across the Atlantic Ocean, which induces higher precipitation in most of the Eurasian extratropics but drought conditions over northern South America and Africa, and parts of the west coast of North America including Mexico and Alaska (Fig. 4d,e, Fig. S2 d,e). Those indices have shown statistically significant negative trends (Table 1), which may alleviate increased fire danger due to slight reduction in North Atlantic SSTs, related to the Atlantic Multidecadal Oscillation (AMO) (Frajka-Williams et al., 2017). The positive correlation between the indices and increased PFI, does not necessarily is associated with human-induced increased fire activity. Wang and Huang (2022) found a decreased fire trend in central South America associated with weakening of the positive Atlantic Multidecadal Oscillation, and subsequently strengthened northeast trade winds and moisture transport from the Amazon.

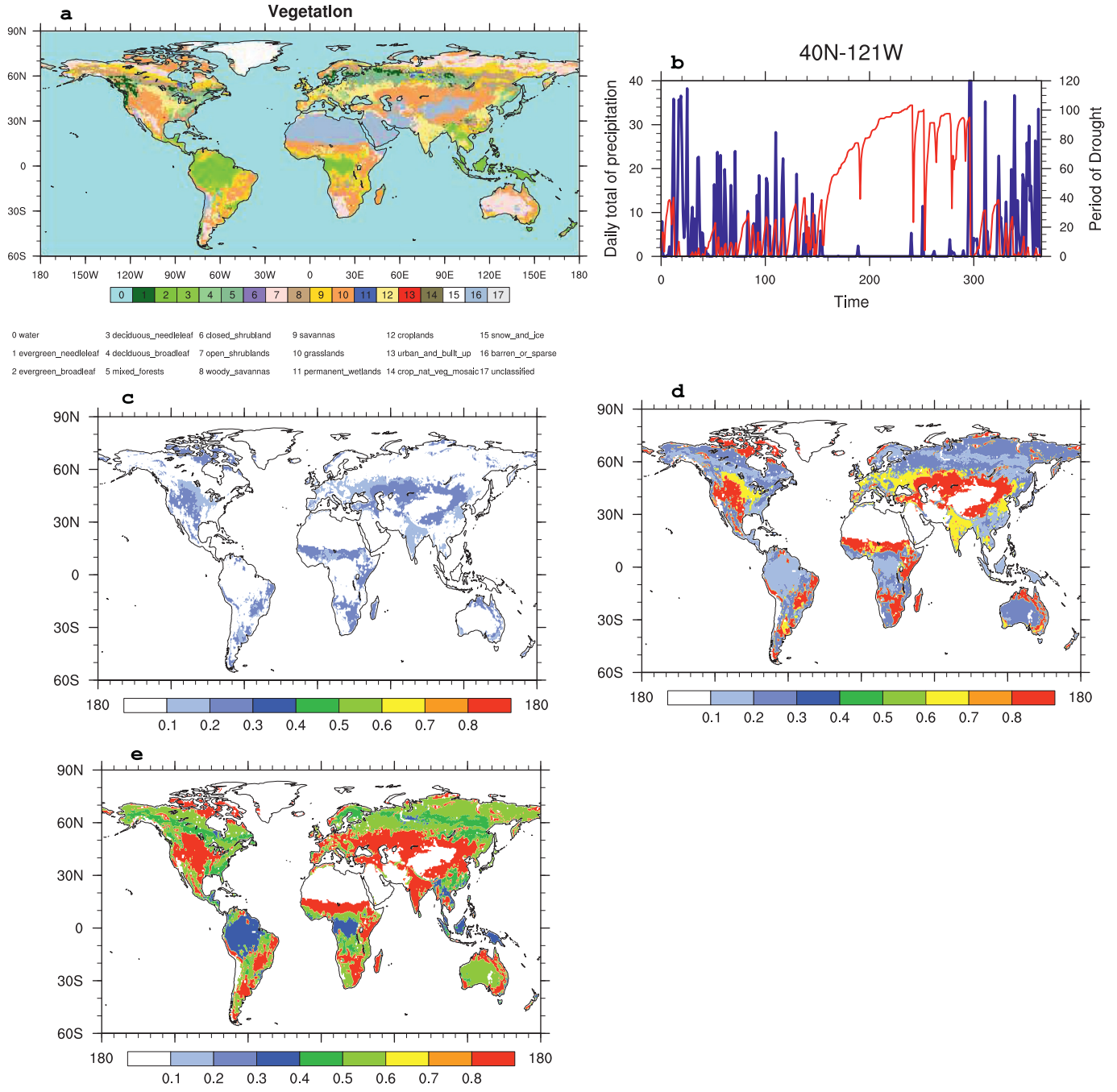

Fig. 3. Dominant vegetation cover (a) and (b) temporal evolution of precipitation (blue line) and DD (red line) for the year 2010 in northern California gridbox (approximately on 40 N, 121 W). (c) to (e) show the PFI component based on DD = 10, 30 and 50, respectively.

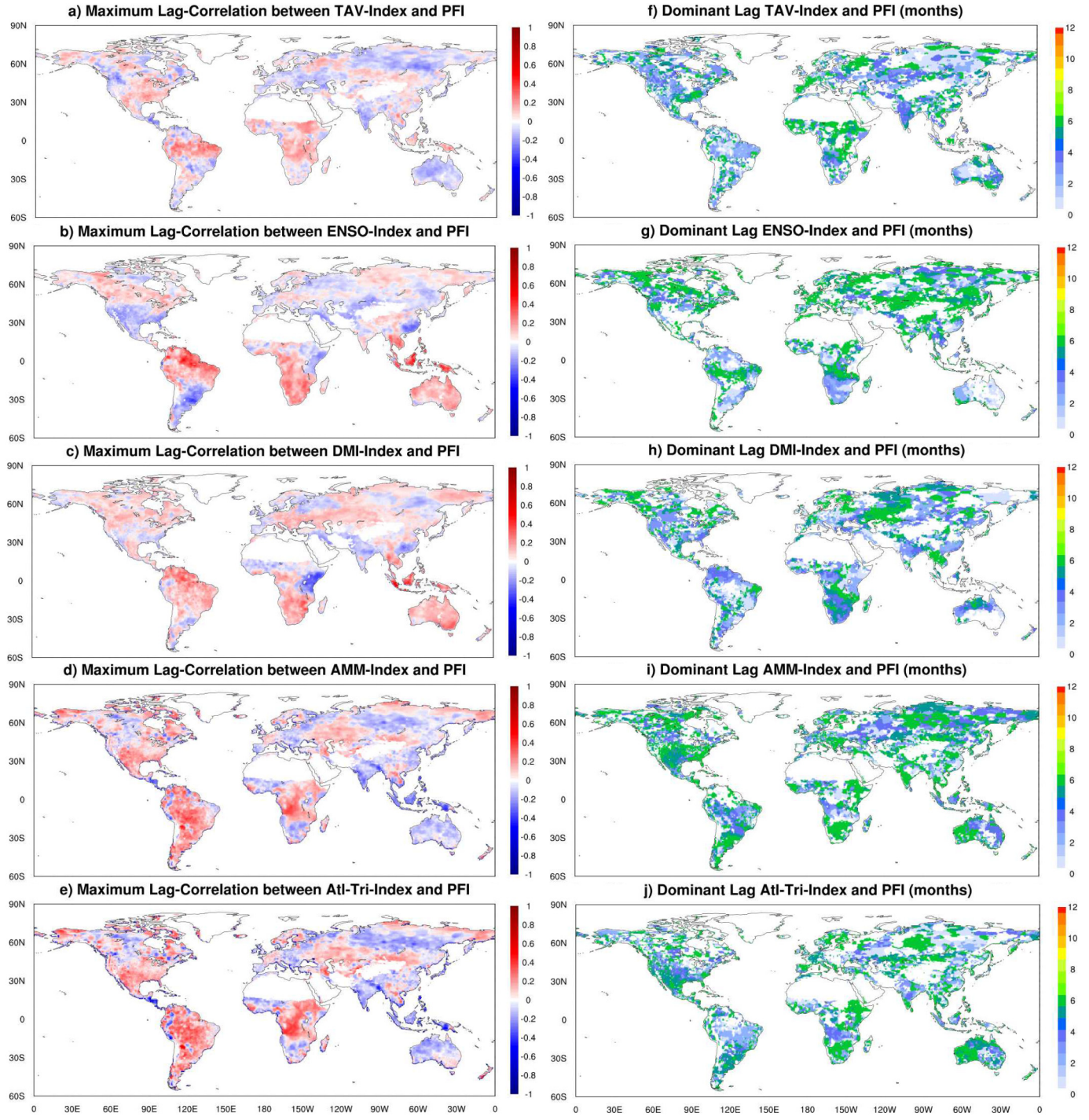

Fig. 4. Maximum lag-correlation between the indices and PFI for (a) TAV, (b) ENSO, (c) DMI, (d) AMM, and (e) Atl-Tri for 1980–2020. The majority of values larger than |0.35| are significant at 95 %. (f) to (j) show the month of maximum correlation based on the vector auto-regressive (VAR) model.

Although, the maximum correlation delivered by these indices displays very similar global pattern, they differ substantially in the Americam continent and across Eurasia (Fig. 4i,j). The AMM is more related to PFI on longer lag, whereas the Atl-Tri maximum correlation is found in lag between 1 and 3 months, with exception of some parts of Africa, Australia and Asia (Fig. 4j). The Atl-Tri is related to North Atlantic SST anomalies that reaches 70°N, whereas the AMM is confined to 32°N. The large oceanic domain of the Atl-Tri is able to induce atmospheric anomalies almost in phase with changes in SST. Teleconnections related to the AMM, on the other hand, take more time to affect surface climate far distant to the source, such as across Eurasia and northern North America.

3.4. Observed fire frequency and oceanic climatic modes

Although several climatological and statistical characteristics of fire danger indices have been evaluated, further analyzes are required to show consistency with hotspot observations and BA. The absence of such investigation makes the previous discussions entirely dependent on meteorological gridded datasets, that without validation against observations, render conclusions to be entirely dependent upon the applied methodology. Thus, the following section addresses quantitatively, the monthly incidence of satellite based-fires associated with changes of oceanic indices, and discusses potential causes for changes in the spatial distribution. All analyses

Table 1
Decadal Mann-Kendall trends and probability (P) of oceanic indices based on ERA5 SST 1980–2020.

Index	ENSO	DMI	TAV	AMM	Atl-Tripole
C/decade	−0.06	0.01	0.00	−0.44	−0.53
P	0.36	0.91	0.44	0.99	0.99

regarding the global oceanic indices are conducting for indices larger than |0.5| standard deviation (Fig. 5). This allows to have a more direct response of fires associated to DMI, TAV, AMM and ENSO. However, this reduces the percentage of fire occurrences with respect to analyses that uses all months throughout the 2001–2020 interval (See Fig. 6).

The majority of fires detected by MODIS are located across the tropics and subtropics but several fires are also observed in North America causing all sort of damage (Figs. 5 and 6). In addition to the local influence of surface conditions such as vegetation and soil moisture, Fig. 5 demonstrates that climate teleconnections related to the oceanic indices modify the frequency of fires in distinct regions.

Despite being previously presented, the AMM and Atl-Tripole are not shown below because due to their decadal variability, during the 2001–2020 period, they have been mostly positive throughout this interval. Therefore, >85 % of fires are predominantly found for AMM^+ and $Atl\text{-}Tripole^+$.

The TAV^+ which is characterized by higher (lower) SST in the northern (southern) tropical Atlantic, is associated with up to 40 % of detected fires

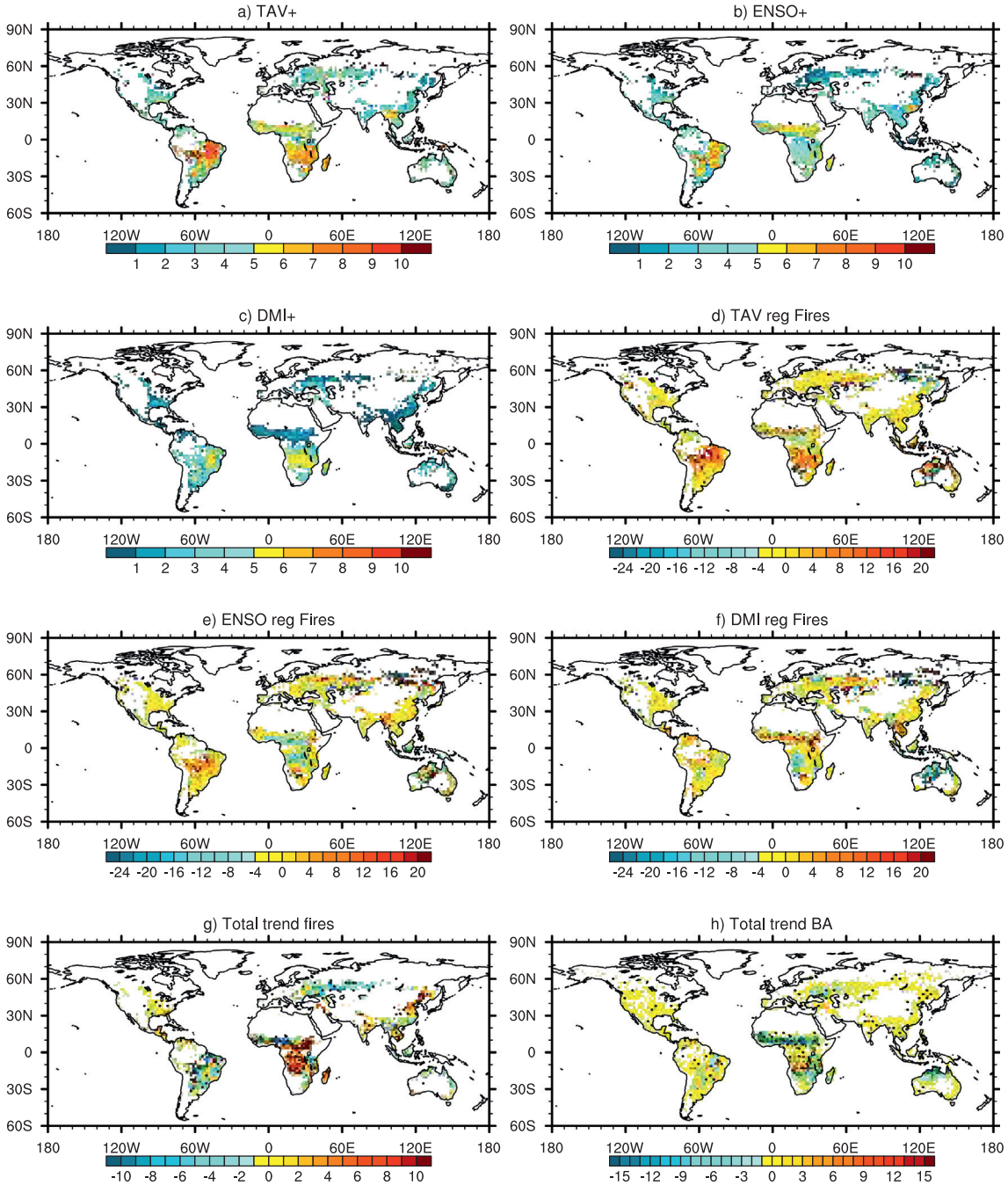

Fig. 5. Percentage of monthly fire occurrences with respect to total amount for indices larger than |0.5| standard deviation. (a) TAV+, (b) ENSO+, (c) DMI+. (d), (e) and (f) show the regression pattern between the indices and the monthly accumulated number of fires for TAV, ENSO and DMI, respectively. (g) and (h) display annual Mann-Kendall trends for the total number of accumulated fires and burned area (km^2) from 2001 to 2020. Note the distinct scaling in the plots.

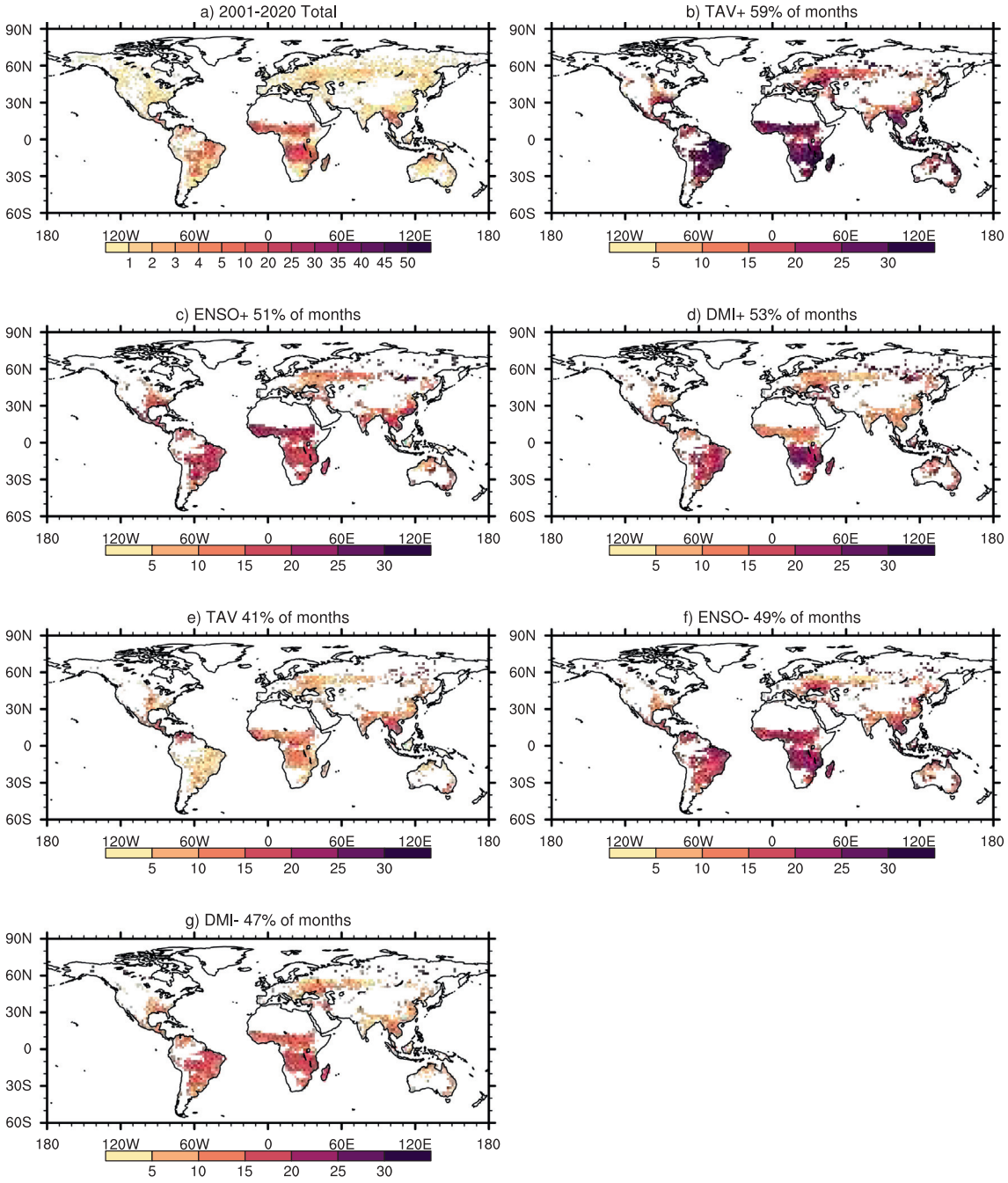

Fig. 6. (a) Total accumulated satellite-detected fires (x10^3) for the 2001–2020. Percentage of fires with respect to total for (b) TAV+, (c) ENSO+, (d) DMI+, (e) TAV+, (f) ENSO- and (g) DMI-. Numbers in the panel titles (b-h) indicate the frequency of occurrence of the event.

from 30°S to 60°N (Fig. 6b) due to a decrease in rainfall (Fig. S2). Fires over large parts of South America and Africa related to extreme TAV^+, with values above |0.5| standard deviation (STD), show that about 8–10 % of fires are found during these intensified conditions (Fig. 5a).

The $ENSO^+$, despite its global influence, shows lesser contribution to total fires in the positive phase (El Niño-like) with respect to the TAV (Fig. 5a,b). However, it is still related with fires in the tropics, contributing significantly to fires in southeastern North America and Asia (Fig. 5c). Over these regions, $ENSO^+$ delivers increased precipitation which can provide additional fuel in the coming months leading to fires. The reduction in the environmental flammability (lower PFI, Fig. 4b) is not sufficient to hamper fire activity. During 2001–2020, ENSO index larger than |0.5| STD has been found in 23 % of the months and its influence should be highlighted in particular across South America, and the Sahelian Africa.

These regions include the Amazonian arc of deforestation in the transition between the rainforest and savannas, and the frontier between the Sahara to the north and the Sudanian savanna to the south.

Both biogeographic regions have experienced high rate of deforestation threatening the livelihood of the ecosystems. Thus, future pattern of ENSO can induce climate conditions able to further accelerate the human-driven and natural clearing of vegetation (Gushchina et al., 2020).

Turning to DMI-fire relationship, an interesting feature emerges over Africa (Figs. 5d, 6d), where in the subtropics DMI^+ is accompanied by higher percentage of fires, but lower concentration in the equatorial belt as compared to the $ENSO^+$ pattern. This is related to the anti-correlated pattern between both indices leading to distinct precipitation distributions (Figs. 5b,c and 6c,d). The DMI^+ due to drought conditions exerts important role in inducing fires in Australia, in particular in the northwestern region

adding to the ENSO$^+$ contribution. Changes in fires in Eurasia and North America related to DMI$^+$ may be also attributed to the global effect of the ENSO and TAV. It should be noted that the ENSO index calculation is based on the tropical Pacific domain, instead of Niño 3.4, 1.2 or Niño 4, thus, current results may differ from other studies, which are based on SST anomalies averaged across much smaller regions.

During the negative phases according to |0.5| STD, which are found for TAV in 17 %, for ENSO 24 % and for DMI in 15 % of the months, the fire incidence reduces in the tropics (not shown), which is mostly related to lower SST in the northern tropical Atlantic. Colder North Atlantic induces the Intertropical Convergence Zone (ITCZ) to predominantly stay over its south position, increasing monsoonal precipitation in East Africa and central South America.

It is discussed below how fires evolve in phase with the oceanic indices based on linear regression. Analyses between those indices and the time evolution of monthly accumulated fires, which is shown by the slope at each grid point for the 2001–2020, demonstrate that the TAV timeseries is associated in South America and parts of equatorial Africa, with temporal increase in satellite-detected fires, whereas negative regression values are found in East Asia and Australia (Fig. 5d). The ENSO supports the TAV pattern in the American Continent and Eurasia (Fig. 5d,e), but they disagree over most of tropical Africa. ENSO primary impacts annual precipitation and leads to drought conditions in large parts of both Africa and South America regions. In Africa, reduced precipitation and high temperatures lead to decline in vegetation cover (Sazib et al., 2020), hence less combustible material is available for the fire season. Most fires in Africa are also related to human actions, and since agricultural activities are weakened due to dry conditions, fire used for clearing bushes are similarly reduced. Turning to Australia, these two indices are related to more frequent incidence of fires in the northwestern region.

The DMI$^+$ is linked to lower fire incidence in Australia, although PFI anomalies indicate positive ratings related to this index (Figs. 5f, 4c). The global analysis limits a close look in particular regions, such as southeastern Australia, where fire have been frequent and related to DMI variability (Wang and Cai, 2020). Fig. 5g,h display the total trend of hotspots and related BA. This primary reveals that trends related to ENSO do not appear in Africa, for which the total trends in fires resemble the fire response to TAV, as shown in Fig. 5d,g. Increases in the incidence of fires in the 2001–2020 period, occur mostly over Africa and southeast Asia, parts of the American Continent and southeast Australia.

Negative trends, are highlighted in central Asia, Sahel, Indonesian Archipelago and South America. These features also depicted by the trends in the BA (Fig. 5h) In the tropics, there is a good match between the fires and BA trends, with increased number of fires resulting in an upward trend of BA.

This is highlighted in eastern North America, southeastern Asia and southern Australia. Most parts of Africa and South America have experienced negative trends, which are not supported by increased fire danger (PFI and FWI). In addition to weather conditions, the occurrence of fires is tightly related to human behavior as well as to policies defined by local authorities.

Earl et al. (2015) analysing anthropogenic influences on global fire from weekly cycles of aerosols demonstrated that these cycles are largely correlated with workdays and notably with days of rest, associated with religious practices. Global environmental principles are also very important to reduce fire activities, and these actions seem to be mainly responsible for the negative trends in South America and Africa, in particular over forested regions.

4. Uncertainties and limitations

Analysis of fire pattern distribution and frequency is a difficult task because involves both human action and environmental conditions. The current study does not include the former effect because it depends upon social levels of environmental conscientization, which is difficult to parameterize.

Influence of human has to be interpreted locally, as it is a matter of collective conscience and engagement of the constituted authorities to define sustainable public policies. Caveats also arise because analyses conducted here are based on reanalyses, blended data and satellite measurements, which may lead to fire danger estimates different than those computed from field observations. Thus, resulting in weaker or stronger link between the oceanic indices and the environmental fire characteristics and hotspots. Lightning induced-fires is other factor that have not been currently considered. However, per se, analyses of fire and lightning require the use of much higher resolution datasets in particular satellite detected hotspots. In this sense, longer time series are not available to investigate the role of oceanic indices and lightning induced-fires.

The understanding of fire patterns and their trends is directly linked to the implementation of fire-weather conditions in fire risk models. The Potential Fire Index (PFI) applied in the current study is able to accurately represent the environmental risk of forest fires, matching in most regions >80 % of satellite detected hotspots, thus, being a useful tool for short-term fire prediction. Analyses conducted here are useful because those climate indices have been forecasted properly and ahead. Thus, by investigating their global impact may help fire agencies and communities to anticipate, and determine regions and municipalities which are more vulnerable in response to climatic impacts of oceanic teleconnections upon fire danger. Results indicate that improvements in prediction of environmental wildfire frequency and severity might be achieved by advanced assessment of the oceanic indices characteristics.

5. Conclusions

Results indicate that seasonal fire forecasts must include vegetation characteristics and climatic conditions induced by teleconnections driven by main modes of oceanic variability, that occur at great distances from the zones of interest. In particular, fire frequency in Africa, North America and South America has been found to be tightly dependent on tropical Atlantic sea surface temperatures.

Fire danger methods, MODIS based-fires and burned area demonstrate at most regions that fire danger indices are able to capture the temporal evolution of satellite measurements, in particular for PFI in Africa and Australia. The understanding of fire frequency and distribution, as well as fire weather trends, requires evaluation that extends beyond the region of occurrence, as demonstrated here. There is an evident impact of oceanic modes of climate variability in inducing an enhancement of environmental conditions conducive to fires, with particular relevance for seasonal forecasts of the spatiotemporal fire characteristics.

Additional work is necessary to connect those anomalies to local levels, under detailed surface characterization of land use and fuel availability. Furthermore, the relationship between observe fires, burned areas and regions under critical fire risk depends on other factors, from lightning strokes to local and Federal policies related to land fire management. Agricultural activities have been modernized in many regions suppressing the use of fire. This leads to negative fire and BA trends but environmental conditions that are still conducive to wildfire. New settlements and expansion of agriculture are occurring in other regions indicating that reduced vulnerability is not sufficient to hamper fire development.

This serves to demonstrate the complexity of attributing causes to the occurrence of wildfires. Large-scale analyses as discussed above, are important because they usefully serve to indicate the environmental fire vulnerability on a global perspective, that should be complemented with the local knowledge to control and avoid fires.

CRediT authorship contribution statement

FJ and DB wrote most of manuscript and analysed results, AS, DA and VS retrieved, processed and generated observed fire and burned area datasets, SH analysed the results and contributed with discussion and programming. All authors reviewed the manuscript.

Funding

FJ thanks the Fulbright Foundation, the Byrd Polar Climate and Research Center (BPCRC), as well as the Brazilian National Council for Scientific and Technological Development (CNPq, grant numbers 442577/2020-6, 305897/2022-5), for financial support. FJ also thanks Dr. Albert Setzer for his major contribution to the PFI formulation. This is the BPCRC publication number C-1624.

Data and materials availability

The FWI is available at https://cwfis.cfs.nrcan.gc.ca/background/summary/fwi and the satellite-based fires at https://earthdata.nasa.gov/earth-observation-data/near-real-time/firms. All additional data and codes used to perform the analysis and generate the figures are available upon request by email to FJ (fjustino@ufv.br).

Declaration of competing interest

The authors declare no competing interests.

Appendix A. Supplementary data

Supplementary data to this article can be found online at https://doi.org/10.1016/j.scitotenv.2023.163397.

References

Ades, M., Adler, R., Allan, R., Allan, R., Anderson, J., Argüez, A., Arosio, C., Augustine, J., Azorin-Molina, C., Barichivich, J., et al., 2020. Global climate. Bull. Am. Meteorol. Soc. 101 (8), S9–S128.

Alexander, M.A., Bladé, I., Newman, M., Lanzante, J.R., Lau, N.C., Scott, J.D., 2002. The atmospheric bridge: the influence of ENSO teleconnections on Air-Sea interaction over the global oceans. J. Clim. 15 (16), 2205–2231. https://doi.org/10.1175/1520-0442(2002).

Black, E., Slingo, J., Sperber, K.R., 2003. An observational study of the relationship between excessively strong short rains in coastal East Africa and Indian Ocean SST. Mon. Weather Rev. 131 (1), 74–94. https://doi.org/10.1175/1520-0493(2003).

Blok, D., Schaepman-Strub, G., Bartholomeus, H., Heijmans, M.M.P.D., Maximov, T.C., Berendse, F., 2011. The response of arctic vegetation to the summer climate: relation between shrub cover, NDVI, surface albedo and temperature. Environ. Res. Lett. 6 (035), 502. https://doi.org/10.1088/1748-9326/6/3/035502.

Burton, C., Betts, R.A., Jones, C.D., Feldpausch, T.R., Cardoso, M., Anderson, L.O., 2020. El niño driven changes in global fire 2015/16. Front. Earth Sci. 8. https://doi.org/10.3389/feart.2020.00199.

Chapman, S., Watson, J.E., Salazar, A., Thatcher, M., McAlpine, C.A., 2017. The impact of urbanization and climate change on urban temperatures: a systematic review. Landsc. Ecol. 32, 1921–1935.

Da Silva, A.S., Justino, F., Setzer, A.W., Avila-Diaz, A., 2021. Vegetation fire activity and the Potential Fire Index (PFIv2) performance in the last two decades (2001–2016). Int. J. Climatol. 41 (S1), E78–E92. https://doi.org/10.1002/joc.6648. https://rmets.onlinelibrary.wiley.com/doi/pdf/10.1002/joc.6648.

DeFries, R.S., Rudel, T., Uriarte, M., Hansen, M., 2010. Deforestation driven by urban population growth and agricultural trade in the twenty-first century. Nat. Geosci. 3 (3), 178–181.

Dowdy, A.J., Mills, G.A., Finkele, K., de Groot, W., 2010. Index sensitivity analysis applied to the Canadian forest fire weather index and the McArthur forest fire danger index. Meteorol. Appl. 17 (3), 298–312. https://doi.org/10.1002/met.170.

Earl, N., Simmonds, I., 2018. Spatial and temporal variability and trends in 2001–2016 global fire activity. J. Geophys. Res. Atmos. 123 (5), 2524–2536.

Earl, N., Simmonds, I., Tapper, N., 2015. Weekly cycles of global fires—associations with religion, wealth and culture, and insights into anthropogenic influences on global climate. Geophys. Res. Lett. 42 (21), 9579–9589. https://doi.org/10.1002/2015GL066383.

Fernandes, K., Baethgen, W., Bernardes, S., Defries, R., DeWitt, D., Goddard, L., Lavado, W., Lee, D., Padoch, C., Pinedo-Vasquez, M., Uriarte, M., 2011. North tropical Atlantic influence on western Amazon fire season variability. Geophys. Res. Lett. 38. https://doi.org/10.1029/2011GL047392.

Frajka-Williams, E., Beaulieu, C., Duchez, A., 2017. Emerging negative Atlantic multidecadal oscillation index in spite of warm subtropics. Sci. Rep. 7 (1), 1–8. https://doi.org/10.1038/s41598-017-11046-x.

Giglio, L., Schroeder, W., Justice, C.O., 2016. The collection 6 MODIS active fire detection algorithm and fire products. Remote Sens. Environ. 178, 31–41.

Gushchina, D., Zheleznova, I., Osipov, A., Olchev, A., 2020. Effect of various types of ENSO events on moisture conditions in the humid and subhumid tropics. Atmosphere 11 (12). https://www.mdpi.com/2073-4433/11/12/1354.

Harris, S., Lucas, C., 2019. Understanding the variability of australianfire weather between 1973 and 2017. PLOS ONE 14, 1–33. https://doi.org/10.1371/journal.pone.0222328 doi: 10.1371/journal.pone.0222328.

Iglesias, V., Balch, J.K., Travis, W.R., 2022. U.S. fires became larger, more frequent, and more widespread in the 2000s. Sci. Adv. 8 (11), eabc0020. https://doi.org/10.1126/sciadv.abc0020.

Jain, P., Castellanos-Acuña, D., Coogan, S., Abatzoglou, J., Flannigan, M., 2021. Observed increases in extreme fire weather driven by atmospheric humidity and temperature. Nat. Clim. Chang. https://doi.org/10.1038/s41558-021-01224-1.

Jolly, W.M., Cochrane, M.A., Freeborn, P.H., Holden, Z.A., Brown, T.J., Williamson, G.J., Bowman, D.M., 2015. Climate-induced variations in global wildfire danger from 1979 to 2013. Nat. Commun. 6 (1), 1–11. https://doi.org/10.1038/ncomms8537.

Justino, F., De Mélo, A., Setzer, A., Sismanoglu, R., Sediyama, G., Ribeiro, G., Machado, J., Sterl, A., 2011. Greenhouse gas induced changes in the fire risk in Brazil in ECHAM5/MPI-OM coupled climate model. Clim. Chang. 106 (2), 285–302. https://doi.org/10.1007/s10584-010-9902-x.

Justino, F., Bromwich, D., Wilson, A., Silva, A., Avila-Diaz, A., Fernandez, A., Rodrigues, J., 2021. Estimates of temporal-spatial variability of wildfire danger across the pan-Arctic and extra-tropics. Environ. Res. Lett. 16 (4). https://doi.org/10.1088/1748-9326/abf0d0.

Justino, F., Bromwich, D.H., Schumacher, V., et al., 2022. Arctic Oscillation and Pacific-North American pattern dominated-modulation of fire danger and wildfire occurrence. npj Clim. Atmos. Sci. 5, 52. https://doi.org/10.1038/s41612-022-00274-2.

Karanasiou, A., Alastuey, A., Amato, F., Renzi, M., Stafoggia, M., Tobias, A., Reche, C., Forastiere, F., Gumy, S., Mudu, P., 2021. Short-term health effects from outdoor exposure to biomass burning emissions: a review. Sci. Total Environ., 146739 https://doi.org/10.1016/j.scitotenv.2021.146739.

Lasslop, G., Kloster, S., 2017. Human impact on wildfires varies between regions and with vegetation productivity. Environ. Res. Lett. 12 (11). https://doi.org/10.1088/1748-9326/aa8c82.

Le Page, Y., Pereira, J.M.C., Trigo, R., da Camara, C., Oom, D., Mota, B., 2008. Global fire activity patterns (1996–2006) and climatic influence: an analysis using the world fire atlas. Atmos. Chem. Phys. 8 (7), 1911–1924. https://doi.org/10.5194/acp-8-1911-2008.

Le Page, Y., Morton, D., Bond-Lamberty, B., Pereira, J.M.C., Hurtt, G., 2015. Hesfire: a global fire model to explore the role of anthropogenic and weather drivers. Biogeosciences 12 (3), 887–903. https://doi.org/10.5194/bg-12-887-2015.

Liu, Z., Alexander, M., 2007. Atmospheric bridge, oceanic tunnel, and global climatic teleconnections. Rev. Geophys. 45 (2). https://doi.org/10.1029/2005RG000172.

Mariani, M., Fletcher, M.S., Holz, A., Nyman, P., 2016. ENSO controls interannual fire activity in southeast Australia. Geophys. Res. Lett. 43 (20), 10,891–10,900. https://doi.org/10.1002/2016GL070572.

Nemani, R.R., Keeling, C.D., Hashimoto, H., Jolly, W.M., Piper, S.C., Tucker, C.J., Myneni, R.B., Running, S.W., 2003. Climate-driven increases in global terrestrial net primary production from 1982 to 1999. Science 300 (5625), 1560–1563. https://doi.org/10.1126/science.1082750.

Ratna, B., Satyaban, Osborn T., Joshi, M., Luterbacher, J., 2020. The influence of Atlantic variability on Asian summer climate is sensitive to the pattern of the sea surface temperature anomaly. J. Clim. 33, 7567–7590. https://doi.org/10.1175/JCLI-D-20-0039.1.

Richardson, D., Black, A., Irving, D., Matear, R., Monselesan, D., Risbey, J., Squire, D., Tozer, C., 2022. Global increase in wildfire potential from compound fire weather and drought. npj Clim. Atmos. Sci. 5, 23. https://doi.org/10.1038/s41612-022-00248-4.

Sazib, N., Mladenova, L.E., Bolten, J.D., 2020. Assessing the impact of ENSO on agriculture over Africa using earth observation data. Front. Sustain. Food Syst., 4 https://doi.org/10.3389/fsufs.2020.509914.

Shi, K., Touge, Y., 2022. Characterization of global wildfire burned area spatiotemporal patterns and underlying climatic causes. Sci. Rep. 12 (1), 1–17. https://doi.org/10.1038/s41598-021-04726-2.

Song, H., Tian, J., Huang, J., Guo, P., Zhang, Z., Wang, J., 2019. Hybrid causality analysis of enso's global impacts on climate variables based on data-driven analytics and climate model simulation. Front. Earth Sci. 7. https://doi.org/10.3389/feart.2019.00233.

Tian, J., Chen, X., Cao, Y., Chen, F., 2022. Satellite observational evidence of contrasting changes in northern eurasian wildfires from 2003 to 2020. Remote Sens. 14 (17), 4180.

Van Wagner, C., Forest, P., 1987. Development and structure of the Canadian forest fireweather index system. Can. For. Serv., Forestry Tech. Rep. Citeseer.

Varga, K., Jones, C., Trugman, A., Carvalho, L.M.V., McLoughlin, N., Seto, D., Thompson, C., Daum, K., 2022. Megafires in a warming world: what wildfire risk factors led to California's largest recorded wildfire. Fire 5 (1). https://doi.org/10.3390/fire5010016.

Wallace, J.M., Gutzler, D.S., 1981. Teleconnections in the geopotential height field during the northern hemisphere winter. Mon. Weather Rev. 109 (4), 784. https://doi.org/10.1175/1520-0493(1981).

Wang, G., Cai, W., 2020. Two-year consecutive concurrences of positive Indian ocean dipole and central pacific el niño preconditioned the 2019/2020 Australian "black summer" bushfires. Geosci. Lett. 7. https://doi.org/10.1186/s40562-020-00168-2.

Wang, Y., Huang, P., 2022. Potential fire risks in south america under anthropogenic forcing hidden by the Atlantic multidecadal oscillation. Nat. Commun. 13 (1), 2437.

Wang, B., Spessa, A.C., Feng, P., Hou, X., Yue, C., Luo, J.J., Ciais, P., Waters, C., Cowie, A., Nolan, R.H., Nikonovas, T., Jin, H., Walshaw, H., Wei, J., Guo, X., Liu, D.L., Yu, Q., 2022a. Extreme fire weather is the major driver of severe bushfires in Southeast Australia. Sci. Bull. 67 (6), 655–664. https://doi.org/10.1016/j.scib.2021.10.001.

Wang, J., Liu, D., Ciais, P., Penuelas, J., 2022b. Decreasing rainfall frequency contributes to earlier leaf onset in northern ecosystems. Nat. Clim. Chang. https://doi.org/10.1038/s41558-022-01285-w.

Wu, D., Zhao, X., Liang, S., Zhou, T., Huang, K., Tang, B., Zhao, W., 2015. Time-lag effects of global vegetation responses to climate change. Glob. Chang. Biol. 21 (9), 3520–3531. https://doi.org/10.1111/gcb.12945.

Yu, Y., Mao, J., Thornton, P.E., Notaro, M., Wullschleger, S.D., Shi, X., Hoffman, F.M., Wang, Y., 2020. Quantifying the drivers and predictability of seasonal changes in African fire. Nat. Commun. 11 (1). https://doi.org/10.1038/s41467-020-16692-w.

Zhang, Z., Wang, L., Xue, N., Du, Z., 2021. Spatiotemporal analysis of active fires in the Arctic region during 2001–2019 and a fire risk assessment model. Fire 4 (3). https://doi.org/10.3390/fire4030057.

Zhao, Z., Lin, Z., Li, F., Rogers, B.M., 2022. Influence of atmospheric teleconnections on interannual variability of arctic-boreal fires. Sci. Total Environ. 838 (156), 550. https://doi.org/10.1016/j.scitotenv.2022.156550.